

LETTERS

Entanglement of single-atom quantum bits at a distance

D. L. Moehring¹, P. Maunz¹, S. Olmschenk¹, K. C. Younge¹, D. N. Matsukevich¹, L.-M. Duan¹ & C. Monroe^{1,2}

Quantum information science involves the storage, manipulation and communication of information encoded in quantum systems, where the phenomena of superposition and entanglement can provide enhancements over what is possible classically^{1,2}. Large-scale quantum information processors require stable and addressable quantum memories, usually in the form of fixed quantum bits (qubits), and a means of transferring and entangling the quantum information between memories that may be separated by macroscopic or even geographic distances. Atomic systems are excellent quantum memories, because appropriate internal electronic states can coherently store qubits over very long timescales. Photons, on the other hand, are the natural platform for the distribution of quantum information between remote qubits, given their ability to traverse large distances with little perturbation. Recently, there has been considerable progress in coupling small samples of atomic gases through photonic channels^{2,3}, including the entanglement between light and atoms^{4,5} and the observation of entanglement signatures between remotely located atomic ensembles^{6–8}. In contrast to atomic ensembles, single-atom quantum memories allow the implementation of conditional quantum gates through photonic channels^{2,9}, a key requirement for quantum computing. Along these lines, individual atoms have been coupled to photons in cavities^{2,10–12}, and trapped atoms have been linked to emitted photons in free space^{13–17}. Here we demonstrate the entanglement of two fixed single-atom quantum memories

separated by one metre. Two remotely located trapped atomic ions each emit a single photon, and the interference and detection of these photons signals the entanglement of the atomic qubits. We characterize the entangled pair by directly measuring qubit correlations with near-perfect detection efficiency. Although this entanglement method is probabilistic, it is still in principle useful for subsequent quantum operations and scalable quantum information applications^{18–20}.

In each of two congeneric radio-frequency ion traps, we trap and laser-cool a single $^{171}\text{Yb}^+$ ion²¹. Each ion is cooled to near the Doppler limit via laser light at 369.5 nm tuned just redward of the $^2\text{S}_{1/2} \leftrightarrow ^2\text{P}_{1/2}$ atomic resonance. The $^2\text{P}_{1/2}$ level also has a decay channel to the $^2\text{D}_{3/2}$ state with a branching ratio of ~ 0.005 (ref. 21). When this decay occurs, the ion is pumped back to the $^2\text{S}_{1/2}$ level via the application of a 935.2 nm laser, as depicted in Fig. 1a. A magnetic field of $B \approx 5.5$ G provides a quantization axis for definition of the photon polarization and the internal atomic qubit levels, stored in the hyperfine levels of the $^2\text{S}_{1/2}$ ground state. This magnetic field also suppresses coherent dark state trapping in the $^2\text{S}_{1/2}$ levels during Doppler cooling and atomic state detection²².

Figure 2 shows a diagram of the relevant energy levels of $^{171}\text{Yb}^+$ along with the step-by-step description of the experimental procedure. After Doppler cooling, pulses of light tuned to the $^2\text{S}_{1/2} \leftrightarrow ^2\text{P}_{1/2}$ transitions initialize, excite and detect the internal states of the ions. First, a 500 ns pulse of light resonant with the $^2\text{S}_{1/2} |F=1\rangle \leftrightarrow ^2\text{P}_{1/2}$

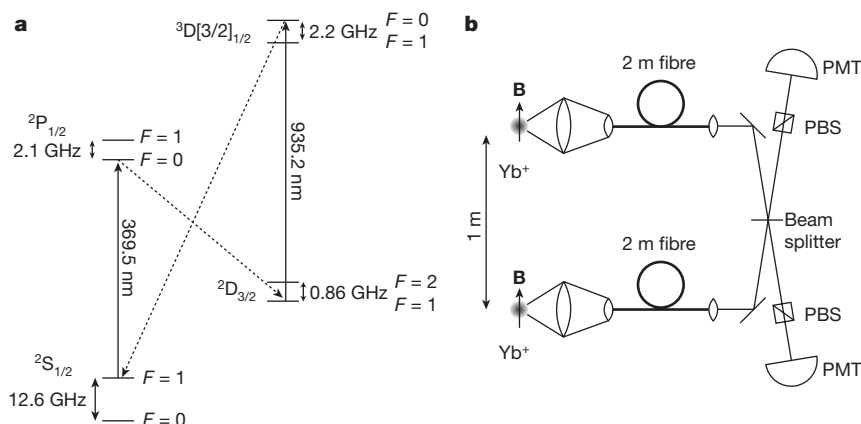


Figure 1 | Experimental apparatus. **a**, Relevant energy levels for $^{171}\text{Yb}^+$. The $^2\text{S}_{1/2} \leftrightarrow ^2\text{P}_{1/2}$ transition is driven by light at 369.5 nm. A frequency-doubled continuous-wave diode laser is used for Doppler cooling, state initialization, and state detection of the ion, whereas the excitation of the ion for single photon generation is accomplished with a mode-locked, frequency-doubled Ti:sapphire laser with a pulse duration of 2 ps (ref. 23). When excited to $^2\text{P}_{1/2}$, the ion can decay to the $^2\text{D}_{3/2}$ level with a branching ratio of ~ 0.005 (ref. 21). A diode laser at 935.2 nm pumps the ion out of this state through the $^3\text{D}[3/2]_{1/2}$ level²¹. **b**, Two ions are trapped in independent vacuum chambers separated by approximately 1 m. Spontaneously emitted photons

from each ion are collected by an $f/2.1$ imaging lens and coupled into single-mode fibres. The polarization of each emitted photon is defined with respect to the applied magnetic field \mathbf{B} oriented perpendicularly to the collection direction. Polarization is maintained through the fibres and can be adjusted via polarization-controlling paddles. The output of each fibre is spatially mode-matched on a 50/50 non-polarizing beam splitter leading to an interference contrast of greater than 97%. Polarizing beam splitters (PBS) are used to filter out the photons of unwanted polarization and the remaining photons are detected on photon-counting PMTs.

¹FOCUS Center and Department of Physics, University of Michigan, Ann Arbor, Michigan 48109-1040, USA. ²JQI and Department of Physics, University of Maryland, College Park, Maryland 20742, USA.

$|F = 1\rangle$ transition prepares each ion in the state $|F, m_F\rangle = |0, 0\rangle$ with more than 99% efficiency²¹. Here F is the total angular momentum and m_F is its projection along the quantization axis. Next, a 2 ps σ^- -polarized laser pulse from a frequency-doubled, mode-locked Ti-sapphire laser excites the ion to the $^2P_{1/2} |1, -1\rangle$ state on a timescale much shorter than the excited state lifetime of $\tau = 8.1$ ns. The ion is prepared in the excited state with an excitation probability of $P_{\text{exc}} \approx 0.5$ (see Methods), and spontaneously decays to either the $^2S_{1/2} |1, -1\rangle$ state while emitting a π -polarized photon or to the $|1, 0\rangle \equiv |\uparrow\rangle$ and $|0, 0\rangle \equiv |\downarrow\rangle$ states while emitting a σ^- -polarized photon (Fig. 2b). The spontaneously emitted photon at 369.5 nm is collected with an $f/2.1$ imaging lens along a direction perpendicular to the quantization axis and is coupled into a single-mode fibre. Along this direction, the polarizations of the π and σ^- decay channels are orthogonal¹³, and the π -polarized photons are filtered out with polarizers. The resulting entangled state between the ion and the photon is $(|\uparrow\rangle|v_\uparrow\rangle - |\downarrow\rangle|v_\downarrow\rangle)/\sqrt{2}$, where $|v_\uparrow\rangle$ and $|v_\downarrow\rangle$ refer to the two resolved frequencies comprising the photonic qubit⁹. The negative sign is a result of the Clebsch–Gordon coefficients, and the two frequency components are separated by the 12.6 GHz ground-state hyperfine splitting.

The output modes of the fibres from each trap are directed onto the two input ports of a 50/50 non-polarizing beam splitter with a transverse spatial mode overlap leading to an interference contrast of more than 97% (Fig. 1b)²³. The photons emerging from the beam splitter are sent through polarizers to filter out the π -polarized decay channel and then to photon-counting photomultiplier tubes (PMTs), each of quantum efficiency $\eta \approx 0.15$.

While the end-to-end coupling efficiency through each fibre is only $\zeta \approx 0.2$ (including the ~ 0.1 dB m^{-1} fibre attenuation), the use of single-mode fibres is essential for the rejection of photons in other spatial modes that would not properly interfere and thereby lower the entanglement fidelity^{15,23}. Temporal mode-matching of photons is accomplished by matching the arrival times of the photon from each ion on the beam splitter to better than 30 ps. Compared to the 8.1 ns photon duration, the remaining temporal mismatch corresponds to a decrease in the mode overlap of under 1%. Finally, spectral matching of the photonic qubits is accomplished by equalizing the magnetic field at the traps to better than 30 mG, resulting in a photonic frequency mismatch of less than 0.2% of the $1/(2\pi\tau) \approx 20$ MHz photon bandwidth. Doppler broadening of the photon emission, from both residual motion of the Doppler-cooled ions and micromotion²⁴, is expected to affect the interference by well under 1%.

When each ion emits a photon into the mode of interest, the quantum state of the system before the photons interact on the

50/50 beam splitter is:

$$\frac{1}{2} [(|\uparrow\rangle_a |v_\uparrow\rangle_a - |\downarrow\rangle_a |v_\downarrow\rangle_a) \otimes (|\uparrow\rangle_b |v_\uparrow\rangle_b - |\downarrow\rangle_b |v_\downarrow\rangle_b)] = \frac{1}{2} (|\Phi^+\rangle_{\text{atom}} |\Phi^+\rangle_{\text{photon}} + |\Phi^-\rangle_{\text{atom}} |\Phi^-\rangle_{\text{photon}} - |\Psi^+\rangle_{\text{atom}} |\Psi^+\rangle_{\text{photon}} - |\Psi^-\rangle_{\text{atom}} |\Psi^-\rangle_{\text{photon}}) \quad (1)$$

where $|\Phi^\pm\rangle_{\text{atom}} = (|\uparrow\rangle_a |\uparrow\rangle_b \pm |\downarrow\rangle_a |\downarrow\rangle_b)/\sqrt{2}$ and $|\Psi^\pm\rangle_{\text{atom}} = (|\uparrow\rangle_a |\downarrow\rangle_b \pm |\downarrow\rangle_a |\uparrow\rangle_b)/\sqrt{2}$ are the maximally entangled Bell states for the ions, with corresponding definitions for the photons. With the photon modes matched on the 50/50 beam splitter, the photons exit on different ports only if they are in the antisymmetric state $|\Psi^\pm\rangle_{\text{photon}} = (|v_\uparrow\rangle_a |v_\downarrow\rangle_b - |v_\downarrow\rangle_a |v_\uparrow\rangle_b)/\sqrt{2}$, respecting the symmetry of the overall photonic wavefunction²⁵. Therefore, coincident photon detection in the two output ports of this beam splitter ideally projects the ions onto $|\Psi^\pm\rangle_{\text{atom}}$ (ref. 26). (This result assumes equal path lengths from each ion to the beam splitter. A simple extension considering differing path lengths can be found in the Methods.) We note that it is the absence of interference between the two different frequency components of each photon that allows for simultaneous detection of a photon on both detectors, because two photons of the same polarization and frequency cannot emerge from the beam splitter along separate paths^{23,27}. Following a heralded entanglement event, near-resonant microwave pulses coherently rotate the trapped ion qubits and prepare them for measurement in different bases. The atomic qubit measurement is performed using standard trapped ion fluorescence techniques with detection efficiency greater than 97% (ref. 21) (Fig. 2c).

We first measure the state of the two ions after the coincident photon detection without microwave rotations. The expected resulting ion–ion entangled state is $|\Psi^-\rangle_{\text{atom}}$, so the atomic wavefunction should have odd parity ($|\uparrow\rangle_a |\downarrow\rangle_b$ or $|\downarrow\rangle_a |\uparrow\rangle_b$). The probability distribution from 274 coincidence detection events is shown in Fig. 3 with a resulting probability of measuring odd parity $p_{\downarrow\uparrow} + p_{\uparrow\downarrow} = 0.78 \pm 0.02$. Here, p_{ab} refers to the probability of measuring the two atomic qubits (ions a and b) in the given spin states.

To verify the entanglement, we repeat the experiment and measure in a rotated basis. Each ion is rotated through a Bloch polar angle of $\theta = \pi/2$ by applying microwave pulses of duration ~ 4 μs near the measured $|\uparrow\rangle_i \leftrightarrow |\downarrow\rangle_i$ frequency splitting of 12.642821 GHz (Fig. 2c). The two atomic qubit transition frequencies are matched to better than 100 Hz and through the use of magnetic-field-insensitive ‘clock states’ as the qubit, the transition frequencies are essentially static over the course of the experiment^{21,28–30}. We vary the relative phase $\Delta\phi = \phi_b - \phi_a$ of the rotations at the two ions by detuning the applied microwaves by 10 kHz from resonance and delaying the microwave pulse on one ion with respect to the other. Here ϕ_i refers to the

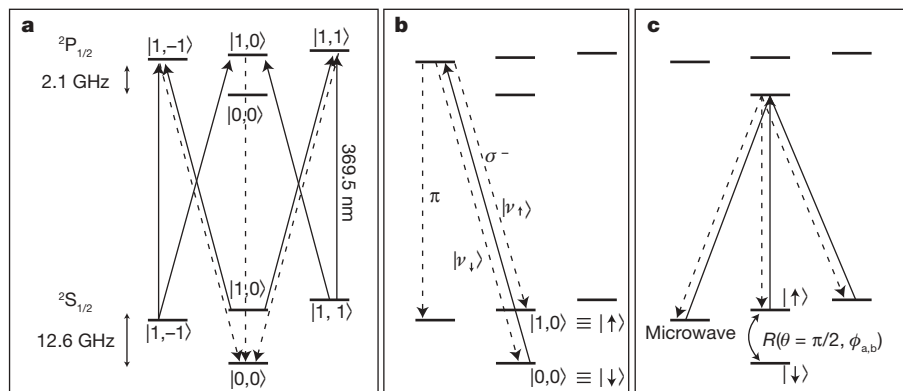


Figure 2 | Experimental procedure. **a**, Each atomic qubit is initialized to the $|F, m_F\rangle = |0, 0\rangle$ hyperfine ground state via a 500 ns optical pumping pulse resonant with the $^2S_{1/2} |F = 1\rangle \leftrightarrow ^2P_{1/2} |F = 1\rangle$ transition including all polarizations. **b**, Each ion is excited with a 2 ps σ^- -polarized optical pulse, resulting in the spontaneous emission of at most a single photon either to the $^2S_{1/2} |1, -1\rangle$ state while emitting a π -polarized photon or to the $|\uparrow\rangle$ and $|\downarrow\rangle$ states while emitting a σ^- -polarized photon. The π -polarized photon is

filtered out by a polarizer resulting in the entangled state $(|\uparrow\rangle|v_\uparrow\rangle - |\downarrow\rangle|v_\downarrow\rangle)/\sqrt{2}$. The steps in **a** and in **b** are repeated on both ions until simultaneous detection occurs on the two PMTs. **c**, Upon simultaneous detection of a photon on each PMT, an optional microwave rotation pulse prepares each atomic qubit for measurement in different bases, followed by measurement of the atomic qubits using standard trapped ion fluorescence techniques, thus resonantly driving all $^2S_{1/2} |F = 1\rangle \leftrightarrow ^2P_{1/2} |F = 0\rangle$ transitions.

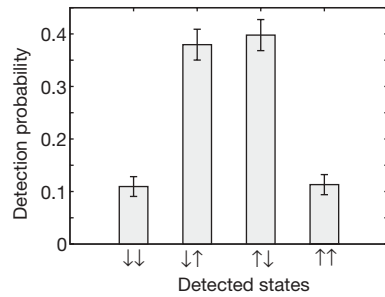


Figure 3 | Unrotated basis results. Measured probabilities in the unrotated basis (no atomic qubit rotation before measurement) conditioned upon coincident detection of photons on each PMT (photon pairs with less than 16 ns detection-time difference). The measured probabilities are $p_{\downarrow\downarrow} = 0.11 \pm 0.02$, $p_{\downarrow\uparrow} = 0.38 \pm 0.03$, $p_{\uparrow\downarrow} = 0.40 \pm 0.03$ and $p_{\uparrow\uparrow} = 0.11 \pm 0.02$, so odd parity is found with a probability of $p_{\downarrow\uparrow} + p_{\uparrow\downarrow} = 0.78 \pm 0.02$. The errors are statistical (standard error) and are collected from 274 coincidence detection events.

microwave phase on ion $i = a, b$ and a 100 μs delay results in a phase difference of $\Delta\phi = 2\pi$. Figure 4 displays the resulting oscillations of the measured atomic qubit parity as a function of the relative phase of the $\pi/2$ rotations. The contrast of this oscillation is directly related to the coherence between $|\downarrow\rangle_a|\uparrow\rangle_b$ and $|\uparrow\rangle_a|\downarrow\rangle_b$.

From these measurements, we calculate a fidelity of $\mathcal{F} = 0.63 \pm 0.03$ and a lower bound on the entanglement of formation to be $\mathcal{E} \geq 0.12 \pm 0.03$, as described in the Methods. The results are limited mainly by dark counts on the PMTs that lead to false events in $\sim 20\%$ of the measured coincidence events. Other factors contributing to the decrease in fidelity include atomic state detection errors ($< 3\%$ for each ion), imperfect mode-matching on the 50/50 beam splitter (3%), mixing of the photon polarizations owing to the non-zero solid angle (1.5% of detected photons result from a $\Delta m_F = 0$ decay), excitations to the wrong atomic state ($\sim 1\%$), and imperfect rotations of the atomic qubit ($\sim 1\%$). Sources of error from imperfections in the optical fibres and magnetic field fluctuations are estimated to affect the measured entanglement by less than 1%.

As mentioned above, the remote-atom entanglement is a probabilistic process. The success probability P in a given trial depends on the efficiency of generating a single photon from each ion in a specific mode and detecting the photons in coincidence. In our excitation scheme (Fig. 2b), each ion has a probability $P_{\text{exc}} \approx 0.5$ of emitting a single photon after the excitation pulse, and $\rho \approx 0.995$ of the emitted photons are at 369.5 nm due to the branching ratio to the $^2D_{3/2}$ state. The detection probability of each photon is given by the light collection solid angle $\Delta\Omega/4\pi \approx 0.02$, coupling efficiency and transmission through the single-mode fibre ζ , transmission through other optical elements $T \approx 0.8$, and the quantum efficiency of the detectors η . In addition, half of the collected photons are π -polarized and are filtered out by the polarizer¹³. Finally, because only the $|\Psi^-\rangle_{\text{photon}}$ state results in the two photons exiting the 50/50 beam splitter in different output ports, there is an additional factor of 1/4 in our success probability: $P = (1/4)[(1/2)\eta\zeta T\rho P_{\text{exc}}(\Delta\Omega/4\pi)]^2 \approx (0.25)[(0.5)(0.15)(0.2)(0.8)(0.995)(0.5)(0.02)]^2 \approx 3.6 \times 10^{-9}$. With an experiment repetition rate of $R \approx 5.5 \times 10^5 \text{ s}^{-1}$, this results in a heralded entanglement event approximately every 8.5 min.

This rate is proportional to the square of the probability of measuring an emitted photon, so improvements in the generation of single photons in the desired mode can significantly increase this yield. Possible improvements include increasing the probability of excitation to unity by using an alternative excitation scheme or collecting the emitted photons along the quantization axis where the radiation strength of the emitted photons is greatest. However, the most substantial improvement would be to place the ion within an optical cavity, which would allow the effective solid angle $\Delta\Omega/4\pi$ to approach unity. Not only would these changes increase the success

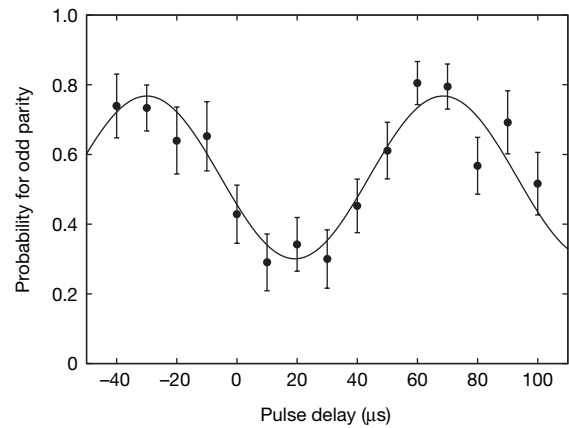


Figure 4 | Rotated bases results. Probability of measuring odd parity of the atomic qubits after rotations on each ion by a polar angle of $\pi/2$ on the Bloch sphere. The horizontal axis corresponds to the delay of the microwave pulse on one ion with respect to the other. Because of the 10 kHz detuning of the applied microwave radiation from resonance, the relative phase of the microwaves pulses, $\Delta\phi = \phi_b - \phi_a$, has a period of 100 μs . The solid line is a fit to the data resulting in a contrast of 0.47 ± 0.05 , where the absolute phase of the interference pattern depends on the difference in microwave transmission lines to each ion. Error bars are statistical (standard error) and the results are from a total of 502 coincidence detection events.

probability, they would also substantially improve the degree of entanglement by lowering the relative contribution of dark count events.

One possible use of this entanglement scheme is a loophole-free Bell inequality violation, with matter qubits prepared in remote locations and measured with high efficiency²⁶. However, successful demonstration of such a violation would require higher entanglement fidelities over much larger distances than that reported here. Additionally, this heralded entanglement could form the basis of a quantum repeater, networking intermediately located ions^{2,18}. Owing to the long coherence and storage times of trapped atomic ions, with the improvements listed above, such a network of remotely entangled ions could be used for scalable quantum computation and communication^{9,18,19}.

METHODS SUMMARY

The use of an ultrafast laser for excitation of the ion to the $^2P_{1/2} |1, -1\rangle$ state is necessary to ensure each ion scatters at most one photon per excitation pulse²³. In our excitation scheme, the broad bandwidth of the ultrafast laser leads to a maximum excitation probability of $P_{\text{exc}} = 50\%$, where the remaining 50% is in a coherent superposition of $|\uparrow\rangle$ and $|\downarrow\rangle$, and does not result in an emitted photon. While P_{exc} can in principle be increased to unity by using alternate atomic states or transitions, the above excitation scheme is sufficient for the creation of photon pairs, and thus for heralded entanglement. The resulting entanglement fidelity and entanglement of formation are calculated from the elements of the density matrix obtained by measuring the ions in the rotated and unrotated bases after the heralded entanglement. The form of the entangled state as given in the text may require an additional phase factor if the path lengths from each ion to the beam splitter are different. In the most general case, coincident photon detection projects the ions onto $(e^{-i\Delta k \Delta x} |\downarrow\rangle_a |\uparrow\rangle_b - |\uparrow\rangle_a |\downarrow\rangle_b) / \sqrt{2}$, where Δk is the difference in wavevectors of the two photon-frequency qubits and Δx is the difference in photon path length from each ion to the beam splitter.

Full Methods and any associated references are available in the online version of the paper at www.nature.com/nature.

Received 17 May; accepted 14 July 2007.

- Nielsen, M. A. & Chuang, I. L. *Quantum Computation and Quantum Information* (Cambridge Univ. Press, Cambridge, UK, 2000).
- Zoller, P. *et al.* Quantum information processing and communication. *Eur. Phys. J. D* **36**, 203–228 (2005).
- Duan, L.-M., Lukin, M. D., Cirac, J. I. & Zoller, P. Long-distance quantum communication with atomic ensembles and linear optics. *Nature* **414**, 413–418 (2001).

4. Sherson, J., Julsgaard, B. & Polzik, E. S. Deterministic atom-light quantum interface. *Adv. At. Mol. Opt. Phys.* **54**, 82–130 (2006).
5. Jenkins, S. D. *et al.* Quantum telecommunication with atomic ensembles. *J. Opt. Soc. Am. B* **24**, 316–323 (2007).
6. Julsgaard, B., Kozhokin, A. & Polzik, E. S. Experimental long-lived entanglement of two macroscopic objects. *Nature* **413**, 400–403 (2001).
7. Chou, C. W. *et al.* Measurement-induced entanglement for excitation stored in remote atomic ensembles. *Nature* **438**, 828–832 (2005).
8. Matsukevich, D. N. *et al.* Entanglement of remote atomic qubits. *Phys. Rev. Lett.* **96**, 030405 (2006).
9. Duan, L.-M. *et al.* Probabilistic quantum gates between remote atoms through interference of optical frequency qubits. *Phys. Rev. A* **76**, 062324 (2006).
10. Berman, P. (ed.) *Cavity Quantum Electrodynamics* (Academic Press, San Diego, California, 1994).
11. McKeever, J. *et al.* Deterministic generation of single photons from one atom trapped in a cavity. *Science* **303**, 1992–1994 (2004).
12. Wilk, T., Webster, S. C., Kuhn, A. & Rempe, G. Single-Atom Single-Photon Quantum Interface. *Science* **317**, 488–490 (2007).
13. Blinov, B. B., Moehring, D. L., Duan, L.-M. & Monroe, C. Observation of entanglement between a single trapped atom and a single photon. *Nature* **428**, 153–157 (2004).
14. Moehring, D. L., Madsen, M. J., Blinov, B. B. & Monroe, C. Experimental Bell inequality violation with an atom and a photon. *Phys. Rev. Lett.* **93**, 090410 (2004).
15. Beugnon, J. *et al.* Quantum interference between two single photons emitted by independently trapped atoms. *Nature* **440**, 779–782 (2006).
16. Volz, J. *et al.* Observation of entanglement of a single photon with a trapped atom. *Phys. Rev. Lett.* **96**, 030404 (2006).
17. Moehring, D. L. *et al.* Quantum networking with photons and trapped atoms. *J. Opt. Soc. Am. B* **24**, 300–315 (2007).
18. Duan, L.-M., Blinov, B. B., Moehring, D. L. & Monroe, C. Scaling trapped ions for quantum computation with probabilistic ion-photon mapping. *Quant. Inf. Comp.* **4**, 165–173 (2004).
19. Duan, L.-M. & Raussendorf, R. Efficient quantum computation with probabilistic quantum gates. *Phys. Rev. Lett.* **95**, 080503 (2005).
20. Barrett, S. D. & Kok, P. Efficient high-fidelity quantum computation using matter qubits and linear optics. *Phys. Rev. A* **71**, 060310(R) (2005).
21. Olmschenk, S. *et al.* Manipulation and detection of a trapped Yb^+ ion hyperfine qubit. Preprint at (<http://arxiv.org/abs/0708.0657>) (2007).
22. Berkeland, D. J. & Boshier, M. G. Destabilization of dark states and optical spectroscopy in Zeeman-degenerate atomic systems. *Phys. Rev. A* **65**, 033413 (2002).
23. Maunz, P., Moehring, D. L., Olmschenk, S., Younge, K. C., Matsukevich, D. N. & Monroe, C. Quantum interference of photon pairs from two remote trapped atomic ions. *Nature Phys.* **3**, 538–541 (2007).
24. Dehmelt, H. Radiofrequency spectroscopy of stored ions. I: Storage. *Adv. At. Mol. Phys.* **3**, 53–72 (1967).
25. Hong, C. K., Ou, Z. Y. & Mandel, L. Measurement of subpicosecond time intervals between two photons by interference. *Phys. Rev. Lett.* **59**, 2044–2046 (1987).
26. Simon, C. & Irvine, W. T. M. Robust long-distance entanglement and a loophole-free Bell test with ions and photons. *Phys. Rev. Lett.* **91**, 110405 (2003).
27. Legero, T., Wilk, T., Kuhn, A. & Rempe, G. Characterization of single photons using two-photon interference. *Adv. At. Mol. Opt. Phys.* **53**, 253–289 (2006).
28. Bollinger, J. J., Heinzen, D. J., Itano, W. M., Gilbert, S. L. & Wineland, D. J. A 303 MHz Frequency Standard based on Trapped Be^+ Ions. *IEEE Trans. Inst. Meas.* **40**, 126–128 (1991).
29. Roos, C. F. *et al.* Bell states of atoms with ultralong lifetimes and their tomographic state analysis. *Phys. Rev. Lett.* **92**, 220402 (2004).
30. Langer, C. *et al.* Long-lived qubit memory using atomic ions. *Phys. Rev. Lett.* **95**, 060502 (2005).

Acknowledgements This work is supported by the National Security Agency and the Disruptive Technology Office under Army Research Office contract, and the National Science Foundation Information Technology Research (ITR) and Physics at the Information Frontier (PIF) programmes.

Author Information Reprints and permissions information is available at www.nature.com/reprints. The authors declare no competing financial interests. Correspondence and requests for materials should be addressed to D.L.M. (david.moehring@mpq.mpg.de).

METHODS

Limits on excitation probability. To ensure that at most a single photon is emitted from each ion following an excitation pulse, it is important to use a laser pulse that is much shorter than the lifetime of the excited state²³. Here, we use a 2 ps laser pulse from a mode-locked, frequency-doubled Ti:sapphire laser that is much shorter than the 8.1 ns excited-state lifetime of the $^2P_{1/2}$ level. This near transform-limited pulse has a bandwidth of ~ 250 GHz which is not only much larger than the $^2P_{1/2}$ linewidth, but also much larger than the $^2S_{1/2}$ hyperfine splitting. Hence, the σ^- -polarized optical pulse that resonantly excites the $^2S_{1/2}$ $|0, 0\rangle$ state to the $^2P_{1/2}$ $|1, -1\rangle$ state is also resonant with the $^2S_{1/2}$ $|1, 0\rangle \leftrightarrow ^2P_{1/2}$ $|1, -1\rangle$ transition³¹. In this three-level lambda system, the largest population which can be transferred to the $|1, -1\rangle$ state when starting from $|0, 0\rangle$ is $P_{\text{exc}} = 50\%$, with the other 50% in an equal superposition of $|0, 0\rangle$ and $|1, 0\rangle$.

In principle, the excitation probability can be improved to unity by preparing an appropriate initial superposition of $|0, 0\rangle$ and $|1, 0\rangle$. Alternatively, different excitation schemes can be adopted¹⁷; for example, exciting to the $^2P_{1/2}$ $|1, -1\rangle$ state from the $^2S_{1/2}$ $|1, -1\rangle$ state via a π -polarized optical pulse.

Phase of entangled state. When considering all phases, the quantum state of the system before interference on the beam splitter is

$$\frac{1}{2} \left[\left(e^{-i\omega_1 t} |\uparrow\rangle_a e^{ik_1 x_a - i\omega_1 t} |v_\uparrow\rangle_a - e^{-i\omega_1 t} |\downarrow\rangle_a e^{ik_1 x_a - i\omega_1 t} |v_\downarrow\rangle_a \right) \otimes \left(e^{-i\omega_1 t} |\uparrow\rangle_b e^{ik_1 x_b - i\omega_1 t} |v_\uparrow\rangle_b - e^{-i\omega_1 t} |\downarrow\rangle_b e^{ik_1 x_b - i\omega_1 t} |v_\downarrow\rangle_b \right) \right] \quad (2)$$

where $\hbar(\omega_\uparrow - \omega_\downarrow)$ and $\hbar(\omega_{v\uparrow} - \omega_{v\downarrow})$ are the energy differences between the two atomic and photonic qubit states, respectively, and x_i is the photon path length from the i th ion to the beam splitter. However, because $\omega_\uparrow + \omega_{v\uparrow} = \omega_\downarrow + \omega_{v\downarrow}$, the equation can be rewritten as:

$$\frac{1}{2} \left[\left(e^{ik_1 x_a} |\uparrow\rangle_a |v_\uparrow\rangle_a - e^{ik_1 x_a} |\downarrow\rangle_a |v_\downarrow\rangle_a \right) \otimes \left(e^{ik_1 x_b} |\uparrow\rangle_b |v_\uparrow\rangle_b - e^{ik_1 x_b} |\downarrow\rangle_b |v_\downarrow\rangle_b \right) \right] \quad (3)$$

The two photons emerge from the beam splitter along separate paths only if they are in the antisymmetric state $|\Psi^-\rangle_{\text{photon}} = (|v_\uparrow\rangle_a |v_\downarrow\rangle_b - |v_\downarrow\rangle_a |v_\uparrow\rangle_b) / \sqrt{2}$. Upon simultaneous photon detection, the ions are projected onto

$$\frac{1}{\sqrt{2}} \left(-|\uparrow\rangle_a |\downarrow\rangle_b + e^{-i\Delta k \Delta x} |\downarrow\rangle_a |\uparrow\rangle_b \right) \quad (4)$$

where $\Delta k \equiv k_{v_\uparrow} - k_{v_\downarrow}$ and $\Delta x \equiv x_a - x_b$. We note that the entanglement is insensitive to fluctuations in the path length at the scale of the optical wavelength^{13,26}. The relative phase appearing in the entangled state of equation (4) is only

sensitive to path length fluctuations compared to the wavelength associated with the frequency difference of the photonic and atomic qubit states $2\pi/\Delta k = c/(\omega_{v_\uparrow} - \omega_{v_\downarrow}) = 2.4$ cm. Stability over this scale is easily achieved.

Fidelity and entanglement of formation. The desired resulting entangled state is $|\Psi^-\rangle_{\text{atom}} = (|\uparrow\rangle_a |\downarrow\rangle_b - |\downarrow\rangle_a |\uparrow\rangle_b) / \sqrt{2}$, so the calculated fidelity is $\mathcal{F} = (\rho_{\uparrow\downarrow, \uparrow\downarrow} + \rho_{\uparrow\downarrow, \uparrow\downarrow}) / 2 + |\rho_{\uparrow\downarrow, \uparrow\downarrow}|$, where $\rho_{ij,kl} = \langle ij|\rho|kl\rangle$ and $i, j, k, l \in (\uparrow, \downarrow)$. The unrotated basis measurements yield $\rho_{\downarrow\downarrow, \downarrow\downarrow}$, $\rho_{\uparrow\downarrow, \uparrow\downarrow}$, $\rho_{\uparrow\downarrow, \uparrow\downarrow}$ and $\rho_{\uparrow\uparrow, \uparrow\uparrow}$ directly. The rotated basis measurements yield $\tilde{\rho}_{\downarrow\downarrow, \downarrow\downarrow}$, $\tilde{\rho}_{\downarrow\downarrow, \uparrow\downarrow}$, $\tilde{\rho}_{\uparrow\downarrow, \uparrow\downarrow}$ and $\tilde{\rho}_{\uparrow\uparrow, \uparrow\uparrow}$, where $\tilde{\rho}_{ij,kl}$ corresponds to the density matrix elements after the applied microwave $\pi/2$ rotations with phase ϕ_a and ϕ_b on the two ions. We find

$$\tilde{\rho}_{\downarrow\downarrow, \downarrow\downarrow} + \tilde{\rho}_{\uparrow\uparrow, \uparrow\uparrow} - \tilde{\rho}_{\uparrow\downarrow, \uparrow\downarrow} - \tilde{\rho}_{\downarrow\uparrow, \downarrow\uparrow} = 2|\rho_{\uparrow\downarrow, \uparrow\downarrow}| \cos(\phi_a - \phi_b) + 2|\rho_{\downarrow\downarrow, \uparrow\uparrow}| \cos(\phi_a + \phi_b) \quad (5)$$

In the experiment, we control the relative phase $\Delta\phi = \phi_b - \phi_a$ between the microwave pulse on each ion, but have no control over the absolute phase of the applied microwaves. Therefore, the measured contrast in the rotated basis measurement comes entirely from the $\rho_{\uparrow\downarrow, \uparrow\downarrow}$ term, with a resulting fidelity $\mathcal{F} = (\rho_{\uparrow\downarrow, \uparrow\downarrow} + \rho_{\uparrow\downarrow, \uparrow\downarrow} + C) / 2 = 0.63 \pm 0.03$, where C is the contrast of the oscillations in Fig. 4.

A lower bound on the entanglement of formation can be calculated by suppressing the unobserved single-qubit coherences (for example, $\rho_{\downarrow\downarrow, \uparrow\uparrow}$ or $\rho_{\uparrow\downarrow, \uparrow\downarrow}$), which cannot increase the entanglement. The resulting density matrix can then be expressed as

$$\begin{array}{cccc} & |\downarrow\rangle_a |\downarrow\rangle_b & |\downarrow\rangle_a |\uparrow\rangle_b & |\uparrow\rangle_a |\downarrow\rangle_b & |\uparrow\rangle_a |\uparrow\rangle_b \\ \begin{array}{l} |\downarrow\rangle_a |\downarrow\rangle_b \\ |\downarrow\rangle_a |\uparrow\rangle_b \\ |\uparrow\rangle_a |\downarrow\rangle_b \\ |\uparrow\rangle_a |\uparrow\rangle_b \end{array} & \begin{pmatrix} 0.11 & & & \\ & 0 & & \\ & & 0.38 & 0.235 \\ & & 0.235 & 0.40 \\ \rho_{\uparrow\downarrow, \uparrow\downarrow} & & & 0 & 0.11 \end{pmatrix} & & & \end{array} \quad (6)$$

From this, the lower bound is numerically calculated using the procedure outlined in references³² and³³, resulting in a concurrence of $\mathcal{C} \geq 0.25 \pm 0.04$ and an entanglement of formation of $\mathcal{E} \geq 0.12 \pm 0.03$.

- Madsen, M. J. *et al.* Ultrafast coherent excitation of a trapped ion qubit for fast gates and photon frequency qubits. *Phys. Rev. Lett.* **97**, 040505 (2006).
- Bennett, C. H., DiVincenzo, D. P., Smolin, J. A. & Wootters, W. K. Mixed-state entanglement and quantum error correction. *Phys. Rev. A* **54**, 3824–3851 (1996).
- Hill, S. & Wootters, W. K. Entanglement of a pair of quantum bits. *Phys. Rev. Lett.* **78**, 5022–5025 (1997).